33rd Annual International Conference of the IEEE EMBS
Boston, Massachusetts USA, August 30 - September 3, 2011

L_1-Regularized Cerenkov Luminescence Tomography With a SP_3 Method and CT Fusion

Jianghong Zhong, Jie Tian*, *Fellow, IEEE*, Xin Yang, *Member, IEEE*, Chenghu Qin, *Member, IEEE*

***Abstract*— Imaging modality of radionuclides has been enriched by an optical approach, Cerenkov luminescence tomography (CLT). Referred to the traditional radionuclide imaging, such as positron emission tomography (PET) or single photon emission computed tomography (SPECT), any incremental improvement of CLT imaging is consistent with the application to information needs. In this contribution, the paper presents an l_1-regularized imaging method for CLT problem. After utilizing the Vavilov-Cerenkov effect via third-order simplified spherical harmonics (SP_3) approximation, we establish the large-scale linear equations in the CLT framework. The derived linear problem is seriously ill-posed, and transformed into an l_1-regularized least squares program. The inverse solution to these equations is the three-dimensional radioisotope recovery data by an interior-point method. In the physical phantom and the *in vivo* mouse experiment, results demonstrate that the proposed technique produces better imaging quality and improves the reconstruction efficacy, compared with those from diffusion approximation with the Tikhonov regularization.**

I. INTRODUCTION

Radioactive tracers for Cerenkov optical imaging will have significant potential for both small animal and clinical imaging. The linear correlation between Cerenkov optical images and positron emission tomography (PET) or single photon emission computed tomography (SPECT) images has been validated as a matter of common knowledge [1], [2], [3]. An accurate three-dimensional Cerenkov tomography with the characteristics of optical imaging has great potential to improve the evolution of tomographic imaging and systems in nuclear medicine. To the best of our knowledge, there were two public papers [4], [5] reported Cerenkov luminescence tomography (CLT) with the diffusion equation (DE) to model *in vivo* Cerenkov photon propagation in today's international academic journals. However, Cerenkov radiation spectrum is weighted toward the ultraviolet and blue bands [6]. The basic prerequisite for the establishment of DE equation will be no longer available because of the ratio of optical scattering and absorption coefficient in tissues [7], [8], [9]. In another aspect, medical isotopes are mainly used for early diagnosis and treatment of diseases. So their distribution is sparse in the body. This characteristics for the optical reconstruction offers the possibility of computation cost saving.

We propose an easy solution to both the above issues: l_1-regularized CLT with the spherical harmonics approximation and CT fusion method. The simplified spherical harmonics (SP_N) method has been developed which requires $(N+1)/2$ equations, where N is the number of Legendre polynomials. SP_N can yield an effective forward model for the Cerenkov light transport in scattering media, considered equivalent to the numerical Monte Carlo (MC) method [10], [11], [12]. After the linear relationship between the measured boundary currents and the unknown light source distribution is established, the attention is paid to sparse signal reconstruction. Kim reported an interior-point method for large-scale l_1-regularized least squares problem [13]. Its performance was illustrated on a magnetic resonance imaging data set. Here, we apply this method and further study its performance in the inverse problem of CLT.

In this study, the performance of l_1-regularized CLT technique through the third-order simplified spherical harmonics (SP_3) approximation and CT fusion is investigated. The paper is organized in the following sequence. In section 2, we formulate the CLT forward and inverse problem in detail. In section 3, the results of physical experiments can draw us to the conclusion that the proposed technique can improve the quality of images. Finally, we will give our discussions and conclude the paper in section 4.

II. METHODS

A. Forward model

The SP_3 method yields transport-like solutions with lowest computational cost in biological tissue compared with SP_N ($N > 3$) [14]. After formulating the time-independent radiation transport equation (RTE) via the SP_3 approximation with the finite element discretization [15], [16], the photon propagation model can be described [12]. The detector readings are obtained with the permissible source region strategy [17] from the exiting partial current J at the tissue boundary, as follows,

$$J = [a(P_{11} - \frac{2}{3}P_{12}) + b(P_{21} - \frac{2}{3}P_{22})]FS = AS. \quad (1)$$

A is the coefficient matrix, and both a and b are constant. Equation (1) is the forward solution used as the linear equations between the measured boundary values and the unknown light source distribution.

This paper is supported by the National Basic Research Program of China (973 Program) under Grant No. 2011CB707700, the Knowledge Innovation Project of the Chinese Academy of Sciences under Grant No.KGCX2-YW-907, the National Natural Science Foundation of China under Grant No.81027002, 81071205, 30970778, 81071129, the Fellowship for Young International Scientists of the Chinese Academy of Sciences under Grant No. 2010Y2GA03.

Intelligent Medical Research Center, Institute of Automation, Chinese Academy of Sciences, Beijing, 100190, China

* Corresponding author: Jie Tian; Telephone: 8610-82628760; Fax: 8610-62527995. tian@ieee.org

B. Inverse model

The inverse problem of CLT is to reconstruct a radioactive light source distribution inside an object, given the surface Cerenkov luminescent distribution. Mathematically, we can define an objective function $f(x)$ as,

$$f(S) \;=\; \|AS - J\|_2^2 + \lambda \|S\|_1, \tag{2}$$

where $\lambda \geq 0$ is the regularization parameter.

Since the inverse problem of CLT is ill-posed with a sparse solution, the regularization is necessary. L_1-regularized least squares typically yields a sparse vector S, which has relatively few nonzero coefficients. In contrast, the solution to the Tikhonov regularization problem by using l_2-regularized typically has all coefficients nonzero. Hence, we apply a specialized interior-point method for solving the large-scale l_1-regularized least squares problem that uses the preconditioned conjugate gradients algorithm to compute the search direction.

According to this method introduced by Kim *et al.* [13], the associated centering problem is to minimize the weighted objective function augmented by the logarithmic barrier for the constraints $S_i \geq 0$

$$\eta \|AS - J\|_2^2 + \eta\lambda \sum_{i=1}^{n} S_i - \sum_{i=1}^{n} \log S_i. \tag{3}$$

Because biological tissues have radioactive substances or not. In other words, the luminescence intensity distribution is a non-negative group. The Newton system for the centering problem is,

$$(2\eta A^T A + D)\Delta S_{newton} \;=\; -g, \tag{4}$$

where D and g were given in [13]. The search direction is computed as an approximate solution to the Newton system, using preconditioned conjugate gradients (PCG). The preconditioner used in the PCG algorithm approximates the Hessian of $\eta\|AS - J\|_2^2$ with its diagonal entries is written as the following form

$$P \;=\; diag(2\eta A^T A) + D. \tag{5}$$

III. Experiments and results

To evaluate the written CLT algorithm in C++, physical experiments were performed. Taking into account the characteristics of CLT reconstruction, we set $\lambda \;=\; 10^{-5}$ with the maximum number of PCG iterations equal to 5000 and its relative error desired equal to 10^{-7}. The initial value of N dimensional column vector S is set to $(0.1, 0.1, \cdots, 0.1)$. We made a comparison between the actual position inside an object and the reconstructed results for the inverse problem by utilizing the measured photon flux density using a CCD camera.

A. Materials and instruments

^{18}F-FDG was kindly provided by Department of Nuclear Medicine, Beijing Union Medical College Hospital.

The same cubic resinous phantom with 20 mm in length was used [18]. The measured optical parameters are listed: the absorption coefficient $\mu_a \;\approx\; 0.02 \times 10^{-2}\, mm^{-1}$, the reduced scattering coefficient $\mu_s' \;\approx\; 106.93 \times 10^{-2}\, mm^{-1}$, $g \;=\; 0.90$ and $n \;=\; 1.37$.

The female Nu/Nu nude mice were purchased from Department of Laboratory Animal Science, Peking University Health Science Center. The optical parameters of the mouse are shown in Table 1. They were the weighted values of the mixed optical spectrum, because there was no optical filter used in this paper.

TABLE I
Optical parameters of the nude mouse [16], [19], $10^{-2}\, mm^{-1}$.

Material	Muscle	Kidney	Bladder	Bone
μ_a	3.20	1.00	68.40	0.24
μ_s'	58.60	83.00	139.00	93.50

High quantum efficiency and low readout noise of our *in vivo* molecular imaging system provide the technical basis for the weak Cerenkov signal acquisition [20], [21]. Our micro-CT system was employed to provide 3D anatomical information in accordance with the normal usage [22]. System control and image processing were carried out on a personal computer with Intel CoreTM 2 Duo Processor 2.33 GHz and 3 GB memory.

B. Physical experiments

The whole physical experiment was performed in a light-tight imaging chamber. The turntable was rotated 360° to have access to the corresponding background and luminescence images. The surface energy distribution was the mean value after subtracting the background noise.

In the phantom experiment, the camera was used to collect the optical images with the aperture number f to 2.8, the binning value equal to 1 and the integration time equal to 100 ms. The homogeneous cube phantom was discretized into 1457 points, 8577 edges, 13565 triangles and 6444 tetrahedrons.

In the *in vivo* experiment, a 21 g mouse was anesthetized by 2% isoflurane was injected with 0.2 mL of Fenestra LC and 11.1 MBq of ^{18}F-FDG via the tail vein. The mouse was scanned by the micro-CT at 30 min after the injection. The dimension of the reconstructed CT data was $400 \times 400 \times 560$ ($0.15 \times 0.15 \times 0.15\ mm^3$ voxel size). 15 min later, we used the camera to collect Cerenkov luminescence images with the aperture number f to 2.8, the binning value equal to 2 and the integration time equal to 3 min. Detailed description of the whole experiment was illustrated in [5]. The reconstructed micro-CT data and four Cerenkov luminescence images were registered and then segmented into 4 major tissues, including muscle, kidney, bladder, and bone. The geometric center of the bladder was (34.60 mm, 14.50 mm, 5.30 mm). We selected part of the micro-CT data along the z axis from the 65^{th} to the 229^{th} slice to reconstruct CLT. It was discredited into 3006 points, 19290 edges, 31868 triangles and 15583 tetrahedrons.

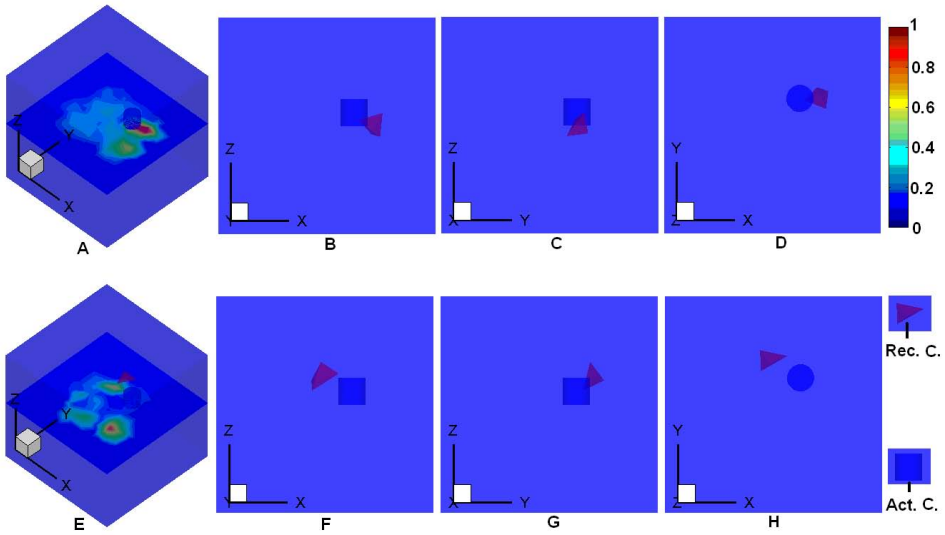

Fig. 1. Comparison between SP_3 model (A to D) and DE model (E to H) in the phantom case. A and E are 3D views with a slice of the flux density distribution when $Z = 10.7mm$; B and F, C and G, D and H are respectively XZ, YZ and XY views. The blue cylinder in each sub figure denotes the real source and the red tetrahedron denotes the reconstructed center with the maximum density. Peak value of the reconstructed flux density is normalized to 1.

C. Source in the phantom

A cylindrical source of 2.5 mm in height and 1.25 mm in radius was centered at (12.5 mm, 12.5 mm, 11.25 mm) in the phantom. The permissible source region (6.5 $mm < x, y, z < 14.5$ mm) was selected, according to the surface light distribution. Based on this data set and SP_3 forward model, the performance of the proposed inverse model (Pro) and that of the famous Tikhonov regularization method (Tik) were investigated. The matrix A used in the last reconstruction procedure was 679×657. The reconstruction results (Fig. 1) were as follows: the recovered maximum light density was 13.50×10^{-9} W/mm^{-2} in Pro and that was 13.70×10^{-9} W/mm^{-2} in Tik; the last reconstruction times were 24.50 s (Pro) and 52.50 s (Tik); the reconstructed centers were (14.20 mm, 12.60 mm, 10.00 mm) with the distance error 2.11 mm (Pro) and (9.63 mm, 14.10 mm, 12.60 mm) with the distance error 3.55 mm (Tik).

D. In vivo source

In the*in vivo* experiment, the 3D mesh and the measured photo flux density distribution on the surface are shown in Fig. 2. According to the surface light, the permissible source region was set to (32 $mm < x <$ 38 mm, 12 $mm < y <$ 17 mm, 3 $mm < z <$ 8 mm). Based on this data set, the performance of the Pro and that of the Tik were investigated. The matrix A used in the last reconstruction procedure was 701×644. Assuming the bladder as a uniform light source owing to the characteristics of the physiological structure and ^{18}F-FDG metabolism, we defined the geometric center of the bladder as the actual light source center. The reconstruction results were as follows: the last reconstruction times were 57.80 s (Pro) and 51.40 s (Tik) with the same regularization parameters as those in the phantom experiment; the reconstructed centers were (33.10 mm, 14.40 mm, 4.64 mm) with the distance error 1.64 mm (Pro) and (33.60 mm, 15.60 mm, 2.58 mm) with the distance error 3.10 mm (Tik).

IV. Discussions and Conclusion

In this paper, we present a simple but efficient approach to CLT. This l_1-regularized CLT with the spherical harmonics approximation and CT fusion method can localize the Cerenkov luminescent source in the mouse. Although the standard SP_3 theory is used in photon transport problems, the research of the Cerenkov photon propagation and CLT inverse problem through the SP_3 and l_1-regularization approach needs further improvement. Mathematically speaking, the model error of all solutions increased in the physical experiments. We performed physical experiments on the phantom by using both the l_1-regularized model and the Tikhonov regularization model. Only the partial current J at the boundary was using, but the distribution of medical isotopes deep inside the medium can be obtained with better accuracy and computational efficiency by the proposed model, comparing with the Tikhonov regularization. Then, the *in vivo* physical experiment was performed. The distance error between reconstructed center and actual center was 1.64 mm by Pro model, while that of Tik model was 3.10 mm. In addition, the proposed method also has a limitation by the use of the parameter η. As the value of η increases, the solution is the sparser, and the reconstructed time is shorter. When the number of nonzero solution is increased to a certain number, and the time cost of the proposed method is almost the same amount of that from the Tikhonov regularization model. Moreover, the permissible regional strategy has reduced the ill-conditioned level for the inverse problem.

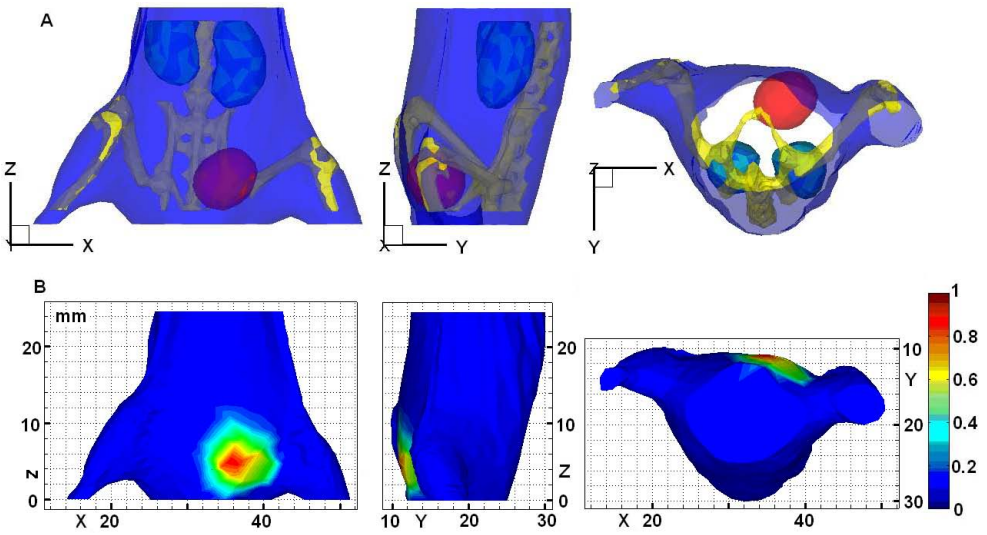

Fig. 2. The 3D finite element mesh with the measured Cerenkov light intensity on the surface. A shows 3D views of the mesh that was composed by 1689 exterior points on the surface. The whole mesh includes the muscle in blue, the bladder in red, the bone in yellow, and the kidney in green. B shows 3D views of the measured flux density distribution on the surface, and peak value of the reconstructed flux density is normalized to 1.

In conclusion, we demonstrated the validation of l_1-regularized CLT with SP_3 approximation for modeling Cerenkov light propagation in biological tissue. Our proposed method can achieve the more transport-like solution. Further, the biodistribution of the medical isotope inside heterogeneous media can be imaged by using the proposed CLT technique without the need of expensive dedicated PET or SPECT. This can facilitate the improvement of radionuclide labeled probes, and has a potential clinical value.

REFERENCES

[1] R. Robertson, M. S. Germannos, C. Li, G. S. Mitchell, S. R. Cherry and M. D. Silva, Optical imaging of Cerenkov light generation from positron-emitting radiotracers, *Phys. Med. Biol.*, vol. 54, 2009, pp N355–N365.

[2] H. Liu, G. Ren, Z. Miao, X. Zhang, X. Tang, P. Han, S. S. Gambhir and Z. Cheng, Molecular optical imaging with radioactive probes, *PLoS One*, vol. 5(e9470), 2010.

[3] A. Ruggiero, J. P. Holland, J. S. Lewis and J. Grimm, Cerenkov luminescence imaging of medical isotopes, *J. Nucl. Med.*, vol. 51, 2010, pp. 1123–1130.

[4] C. Li, G. Mitchell, and S. Cherry, Cerenkov luminescence tomography for small animal imaging, *Opt. Lett.*, vol. 35, 2010, pp. 1109–1111.

[5] J. Zhong, C. Qin, X. Yang, S. Zhu, X. Zhang, and J. Tian, Cerenkov luminescence tomography for in vivo radiopharmaceutical imaging, *Int. J. Biomed. Imaging*, vol. 2011(641618), 2011.

[6] M. A. Lewis, V. D. Kodibagkar, O. K. Öz, and R. P. Mason, On the potential for molecular imaging with Cerenkov luminescence, *Opt. Lett.*, vol. 35, 2010, pp. 3889–3891.

[7] S. R. Arridge, Optical tomography in medical imaging, *Inverse Probl.*, vol. 15, 1999, pp. R41–R93.

[8] A. M. Smith, M. C. Mancini, and S. Nie, Second window for in vivo imaging, *Nat. Nanotechnol*, vol. 4, 2009, pp. 710–711.

[9] A. D. Klose, B. J. Beattieb, H. Dehghanic, L. Vider, C. Le, V. Ponomarev, and R. Blasberg, In vivo bioluminescence tomography with a blocking-off finite-difference SP_3 method and MRI/CT coregistration, *Med. Phys.*, vol. 37, 2010, pp. 329–338.

[10] A. D. Klose, The forward and inverse problem in tissue optics based on the radiative transfer equation: a brief review, *J. Quant. Spectrosc. Radiat. Transf.*, vol. 111, 2010, pp. 1852–1853.

[11] J. Zhong, J. Tian, X. Yang, and C. Qin, Forward model of Cerenkov luminescence tomography with the third-order simplified spherical harmonics approximation, *in Proceedings of SPIE Symposium on Medical Imaging 2011*, Lake Buena Vista, Florida, USA 2011, vol. 7961.

[12] J. Zhong, J. Tian, X. Yang, and C. Qin, Whole-body Cerenkov luminescence tomography with the finite element SP_3 method, *Ann. Biomed. Eng.* vol. 39, 2011, pp. 1728–1735.

[13] S. Kim, K. Koh, M. Lustig, S. Boyd, and D. Gorinevsky, An interior-point method for large-scale l_1-regularized least squares, *IEEE J. Sel. Top. Sign. Proces.*, vol. 1, 2007, pp. 606–617.

[14] Y. Lu, B. Zhu, H. Shen, J. C. Rasmussen, G. Wang, and E. M. Sevick-Muraca, A parallel adaptive finite element simplified spherical harmonics approximation solver for frequency domain fluorescence molecular imaging, *Phys. Med. Biol.*, vol. 55, 2010, pp. 4625–4645.

[15] A. D. Klose and E. W. Larsen, Light transport in biological tissue based on the simplified spherical harmonics equations, *J. Comput. Phys.*, vol. 220, 2006, pp. 441–470.

[16] K. Liu, Y. Lu, J. Tian, C. Qin, X. Yang, S. Zhu, X. Yang, Q. Gao, and D. Han, Evaluation of the simplified spherical harmonics approximation in bioluminescence tomography through heterogeneous mouse models, *Opt. Express*, vol. 18, 2010, pp. 20988–21002.

[17] W. Cong, G. Wang, D. Kumar, Y. Liu, M. Jiang, L. V. Wang, E. A. Hoffman, G. McLennan, P. B. McCray, J. Zabner, and A. Cong, Practical reconstruction method for bioluminescence tomography, *Opt. Express*, vol. 13, 2005, pp. 6756–6771.

[18] B. Zhang, X. Yang, C. Qin, D. Liu, S. Zhu, J. Feng, L. Sun, K. Liu, D. Han, X. Ma, X. Zhang, J. Zhong, X. Li, X. Yang, and J. Tian, A trust region method in adaptive finite element framework for bioluminescence tomography, *Opt. Express*, vol. 18, 2010, pp. 6477–6491.

[19] J. Xu, H. Wei, G. Wu, B. He, and W. Zhang, Differential diagnosis of human normal bladderand bladder cancer tissues by utilizing optical properties of tissues in vitro, *Acta Laser Biol. Sin.*, vol. 18, 2006, pp. 520–524.

[20] J. Tian, J. Bai, X.P. Yan, S.L, Bao, Y.H. Li, W. Liang, and X. Yang, Multimodality molecular imaging, *IEEE Eng. Med. and Biol. Mag.*, vol. 27, 2008, pp 48–57.

[21] C. Qin, J. Tian, X. Yang, K. Liu, G. Yan, J. Feng, Y. Lv, and M. Xu, Galerkin-based meshless methods for photon transport in the biological tissue, *Opt. Express*, vol. 16, 2008, pp 20317–20333.

[22] S. Zhu, J. Tian, G. Yan, C. Qin, and J. Feng, Cone beam micro-CT system for small animal imaging and performance evaluation, *Int. J. Biomed. Imaging*, vol. 2009(960573), 2009.